Depth–Depth Matching of Virtual and Real Images for a Surgical Navigation System

Hiroshi Noborio[1], Katsuhiko Onishi[1], Masanao Koeda[1], Kaoru Watanabe[1], and Miho Asano[2]
[1]Department of Computer Science, Osaka Electro-Communication University, Osaka, Japan
[2]Preemptive Medicine and Lifestyle-Related Disease Research Center, Kyoto University Hospital, Kyoto, Japan
Email: nobori@osakac.ac.jp, masano@kuhp.kyoto-u.ac.jp

***Abstract*—We propose a surgical navigation system aimed at conducting Depth–Depth Matching (DDM) between virtual and real organ images. The depth image of virtual organs modeled using stereolithography data derived from the Z-buffer of a GPU. In contrast, the depth image of real organs is obtained through an arbitrary depth camera. Therefore, in DDM, we need only non-combinatorial *L* subtractions and additions between virtual and real 2D depth images with pixel number of *L*, which is approximately 100,000. The most popular Iterative Closest Point (ICP) algorithm in the point cloud library consumes a considerable amount of time for checking the coincidence of two kinds of point clouds of whole organs. This could be because (1) the ICP needs combinatorial $M \times N$ calculation of the Euclidean distances of 3D cloud points (where *M* and *N* are usually near 100,000) and (2) considering that a real organ is obstructed by the patient's body, the directions from which it is captured by a camera are restricted to the top view or near a shadowless lamp.**

***Index Terms*—Digital Imaging and Communications in Medicine (DICOM), surgical navigation, depth–depth matching, Z-buffer, Stereolithography (STL), Cavitron Ultrasonic Surgical Aspirator (CUSA) scalpel**

I. Introduction

Since 2013, we have been developing a system for liver surgical navigation. Surgical navigation has been gaining considerable interest in the fields of orthopedic surgery, plastic surgery, forming surgery, neurosurgery, kidney surgery, liver surgery, and so on (Table I).

TABLE I. Types of Surgical Navigations

Surgery type	Deformability	Position precision	Orientation precision
Orthopedic surgery	Negligible	Negligible	Negligible
Plastic surgery	None	None	None
Neurosurgery	Partially	A few	A few
Kidney surgery	A few	Large	Large
Liver surgery	Large	Large	Large

First, many studies have reported on navigation results in orthopedic surgery [1]. In comparison, surgical navigation for plastic surgery can easily be dealt with because its main target is bone, the structure and kinematics of which are geometrically fixed. Therefore, construction of a navigation system is relatively easy [2].

Finally, neuro-navigation is also stable as a brain is completely covered by the skull even though the brain itself is slightly deformed. The neuro-navigation is mostly a developing field of study [3], and consequently, some commercialized surgical navigation systems, such as the StealthStation™ (provided by the Medtronic Co.), have been already developed. This system has an intuitive interface, improved patient-registration software, and advanced visualization to navigate neurosurgery procedures.

However, such a type of brain navigation currently faces two serious problems:

(1) The coincidences between real and virtual organs
(2) The identification of movement and deformation of a real organ

In this study, we focused on problem (1). Section II describes a real organ and its virtual counterpart. In addition, we illustrate how to obtain a virtual organ and then build its replica in reality. Then, in Section III, we briefly overview the history of related research, including a 3D stereo [4] and Simultaneous Localization and Mapping (SLAM) [5]-[15]. In particular, we focus on two modern methods: Iterative Closest Point (ICP) in the Point Cloud Library (PCL) [16]-[24] and our Depth–Depth Matching (DDM). In Section IV, we explain DDM theoretically and experimentally [25]-[35]. Finally, Section V briefly summarizes our research.

II. Virtual and Real Organs Used in This Research

By using the following algorithms, we initially captured the patient's liver, its blood vessels, and tumors through MRI- or CT-scan-based Digital Imaging and Communication in Medicine (DICOM) data. Then, we converted volumes of the liver, its blood vessels, and tumors into several STL polyhedrons by using a 3D slicer (Slicer), as shown in Fig. 1. This software is an open-source software package for image analysis [7]-[8] and scientific visualization. The STL is employed rapidly calculate a depth image by using the GPU's Z-buffer and

Manuscript received December 11, 2020; revised February 20, 2021.

doi: 10.18178/ijpmbs.10.2.40-48

to maintain the visual quality. Based on the STL data, we then constructed a plastic replica of the real liver by using a 3D printer (Fig. 2).

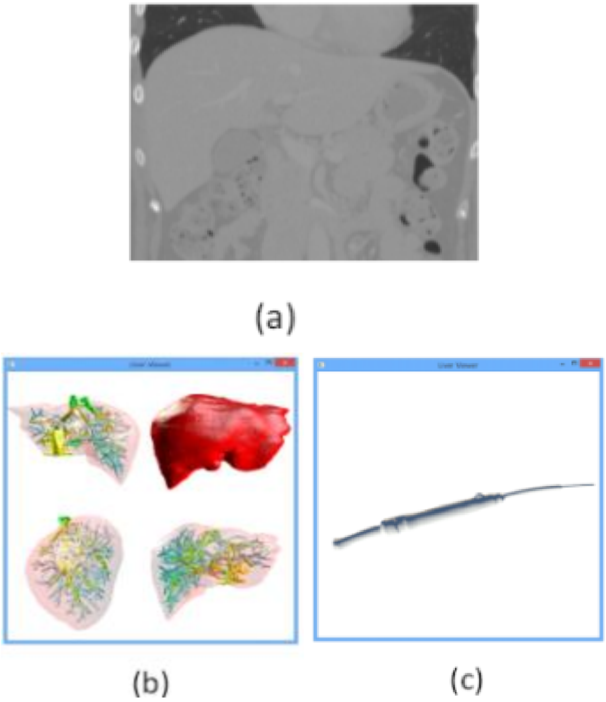

Figure 1. Liver DICOM data; (b) whole liver, arteries, veins, and portal vein STL; and (c) scalpel CUSA (Source: Noborio [36] (2016)).

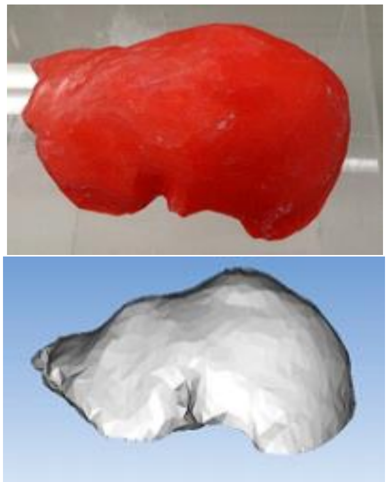

Figure 2. Vertical scale of liver 13cm, horizontal scale of liver 25cm. Upper: STL-formatted polyhedron liver. Lower: its 3D-printed liver replica (Source: Koeda [15] (2019)).

III. Brief History of Replicating a Real Organ Based on Its Virtual Counterpart

In almost all the navigators, people use the 3D mechanical or 2D nonmechanical probe with ultrasonic sensors. However, owing to the low image resolution of the ultrasonic sensor, we cannot detect the orientation, position, and shape of a real liver to precisely navigate it during surgery. Therefore, surgeons can capture the motions of translation and rotation of a real liver and its deformation by using the stereo vision of a 3D camera with real markers. However, we could locate any artificial markers on a real liver because of some damages to the liver due to surgery (Fig. 3).

Figure 3. (a) Pig liver captured by MRI; (b) STL polyhedron converted from DICOM of pig liver. (c) Many active landmarks on a pig liver. (d) Scraper with many landmarks during the surgery of the pig. This experiment was conducted in Kobe Medical Device Development Center (MEDDEC).

Therefore, we selected the SLAM technique to precisely identify the orientation, position, and shape of the real liver by using not real markers but artificially selected markers [9]-[11]. The SLAM technique identifies the surrounding environment’s shape and estimates its orientation and position according to the shape data. In our system, we used ORB-SLAM2 [12], which is partially modified, as the SLAM library, in which three threads of local mapping, loop closing, and tracking run in parallel. In the tracking thread, the orientation and position of the camera is estimated by tracking the image features of oriented FAST and rotated BRIEF (ORB) [13] in the input videos. The positions of a global map and camera are displayed in the local mapping thread. The loop closing thread eliminates the accumulation of the camera position and orientation error. However, during some surgeries, we could not sufficiently test the precisions of the translation and orientation movements of the organ [14] (Fig. 4).

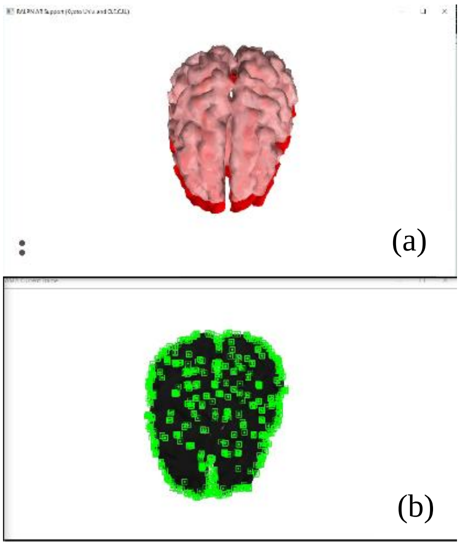

Figure 4. (a) Passive landmarks selected by SLAM on the real brain. (b) A real liver colored by red is traced with respect to its virtual liver colored in pink by using movements of passive landmarks (Source: Koeda [15] (2019)).

IV. COMPARISON BETWEEN DDM AND ICP

In this study, we developed a new liver surgery navigation system based on the key concept DDM of virtual and real liver images (Fig. 5). In general, in surgical navigation, most of the liver (organ) is covered by the patient's body, and only its narrow, open surgical area gradually changes. In this study, we use the shape of the liver incision, which was photographed in one direction from a shadowless lamp and its surroundings, as a landmark for tracking. The change in the shape of the incision at each sampling time was used as a landmark for the virtual liver (organ) to follow the actual liver (organ). This is the idea of DDM of the virtual depth image and the real depth image of the surgical aperture.

In succession, in order to match this virtual liver image with the real liver image, we search for the orientation and position of the virtual liver in 6-DOF (3 parallel and 3 rotational components) space of 3D Euclidean coordinates. In this search, the DDT match is checked in a huge number of neighboring directions to move the virtual liver. The depth image of the virtual liver modeled with STL data is derived from the GPU's Z-buffer. In contrast, the depth image of the real liver is taken by an arbitrary depth camera. Therefore, our DDM technique requires only K × L subtraction between the virtual depth and the real depth in K × L image pixels (where K and L are chosen for any depth camera (Fig. 6). Both values are usually close to 1000).

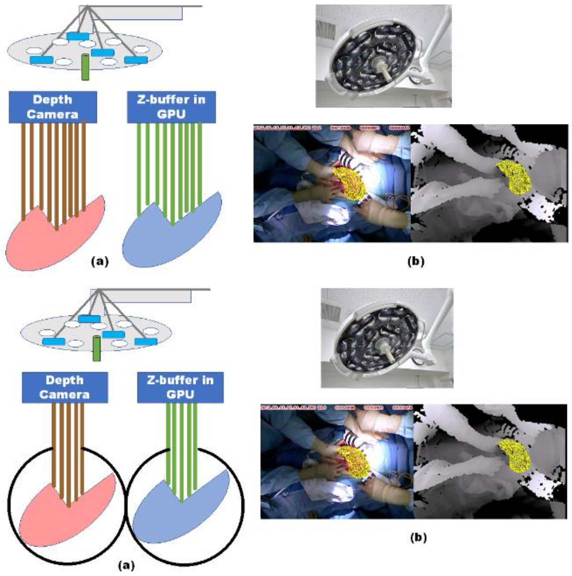

Figure 5. By minimizing the sum of square differences between real and virtual depths in all the pixels, we are seeking for overlapping position and orientation between real and virtual livers. Uppers: No-obstruction case. Bottoms: Obstruction case.

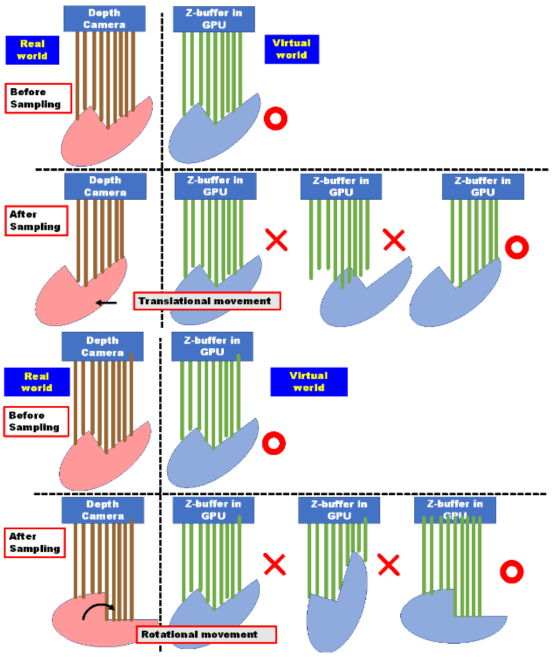

Figure 6. DDM in 3D translation movement. (Bottom) DDM in 3D orientation movement.

This computation is relatively faster than using the ICP algorithm, which is the most popular in PCL for checking the agreement between two different point clouds of all objects. ICP is relatively time-consuming because it requires the computation of M × N combinations of 3D Euclidean distances (M and N are usually close to 100,000; Fig. 7). 2D depth addition and subtraction is relatively faster than the Euclidean distance computation of 3D cloud points (Table II).

TABLE II. COMPARISON BETWEEN DDM AND ICP

	DDM	ICP
View area	2D part based on occlusion	3D space
Number of calculations	Sequential at each pixel	Combination of points in two crowds
Calculation method	Subtraction	Multiplication for Euclidean distance
Number of cameras	One	Multiple

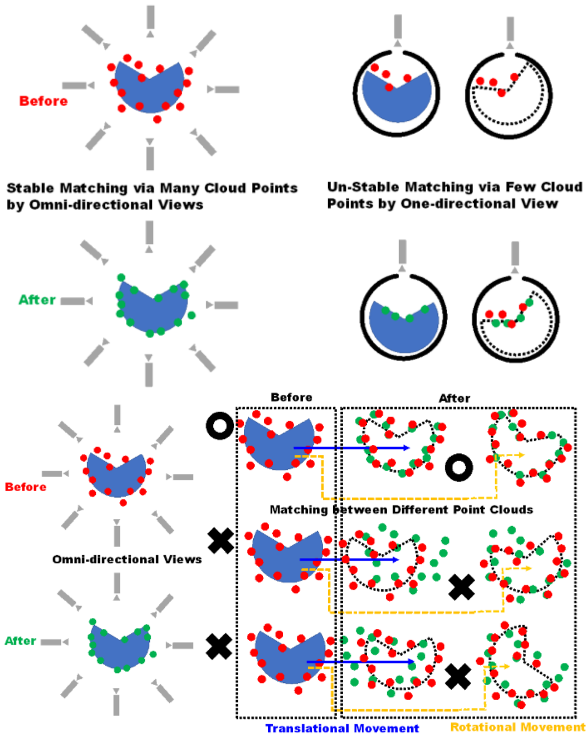

Figure 7. Upper: Matching between two crowds based on the combinational shortest Euclidean distance calculation is very hard because the number of crowd points is too large. Bottom: Correspondence between two crowds becomes failure because the number of crowd points is too small.

V. DDM TECHNIQUE AND ITS APPLICATIONS

Our concept of DDM has been explained in our previous study [25]. The main benefit of DDM is to identify translational and orientational movements by using a specified organ shape. Thus, the cutting shape of an organ or its tumor and blood vessels by a scalpel can easily be achieved by using DDM.

Before using DDM, we should adjust the initialization such that virtual- and real-depth images coincide with each other by using a visual initial identification tool. By using the tool, we can precisely overlap a virtual organ with its real counterpart by watching pixel colors in the depth image (Fig. 8). For each pixel, we can identify the difference between virtual and real depths [26].

Many studies have used several kinds of steepest descendent algorithms for selecting the best neighbor position/orientation to move [27], [28] (Fig. 9). We propose a steepest descendent algorithm to select neighbors, whose numbers are defined by six DOF with 1–3 neighbors and 2 positive- and negative-direction candidates or the presence of 3^6–1, 5^6–1, and 7^6–1 candidates around the present candidate (Fig. 10). Finally, as Six DOF consist of three translational degrees and three rotational degrees, our algorithm is designed for selecting the best translational neighbor point from one 3D space and independently selecting the best orientation neighbor point from the other 3D space [27]-[28] (Fig. 11).

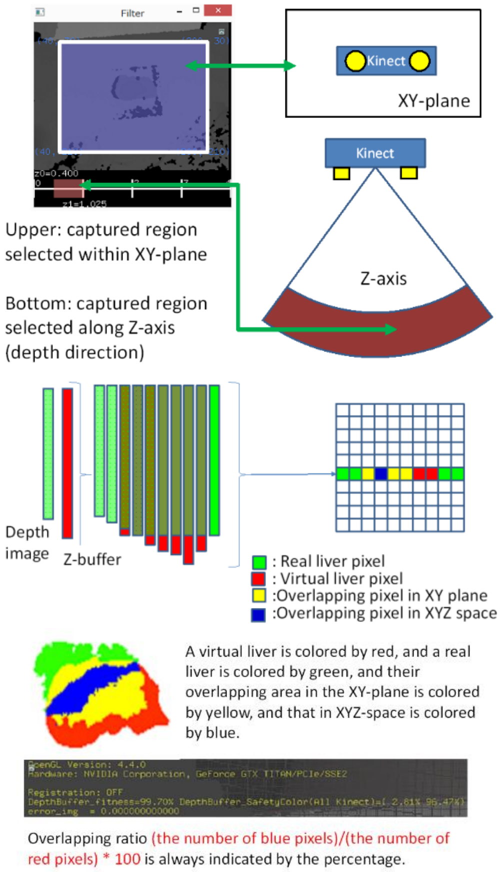

Figure 8. By using the color image, we can precisely overlap a virtual organ with its real organ by changing from green and red to blue via yellow (Source: Noborio [26] (2015)).

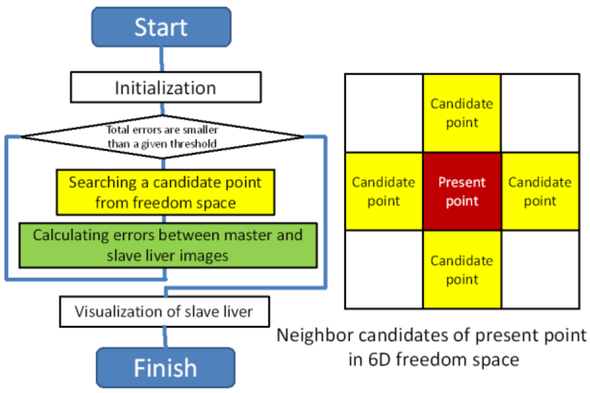

Figure 9. Flowchart of our position and orientation registration method based on digital neighbours (Source: Noborio [28] (2014)).

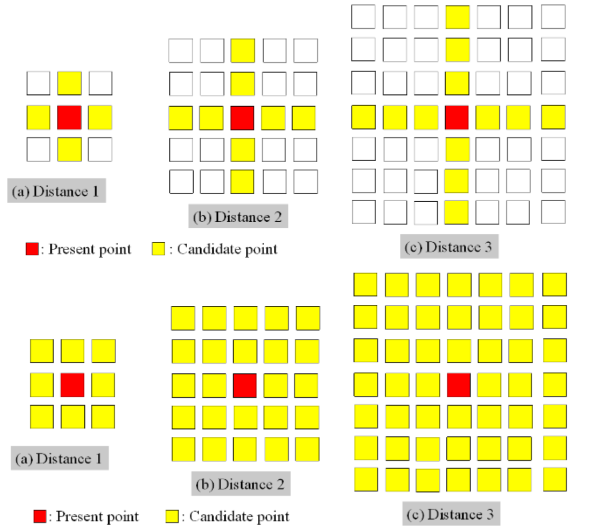

Figure 10. The least descendent algorithm always selects the best neighbors of the present points (=position/orientation) by using the evaluation value. (a), (b), (c), the upper panels show a 1 DOF search space with distances of 1, 2, and 3, respectively. The bottom panels show 6 DOF search space with distances of 1, 2, and 3, respectively (Source: Watanabe [28] (2015)).

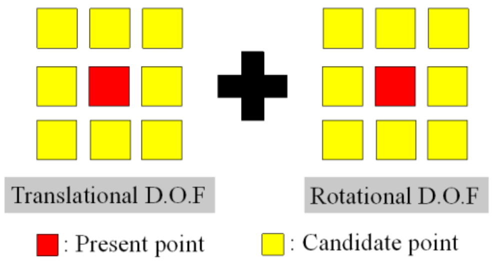

Figure 11. The least descendent algorithm always selects the best points neighboring the present point by using the evaluation value. This figure shows three translational DOF and three rotational DOF search spaces, with distance of 1 (Source: Watanabe [28] (2015)).

Simultaneously, images are selected as the minimum, median, or average values in their distribution. In addition, the number of images, *M*, is simultaneously changed to 10, 50, and 100, and the number of pixels, *N*, is selected randomly. As a result, when using the algorithm with 26 (=3^3-1) or 728 (=9^3-1) neighbors, the median-image-average-pixel type of the DDM algorithms is better than that of the others for all the combinations of *M* and *N* with respect to speed and accuracy. In particular, the combinations of (*M*, *N*) = (10,100) and (50,10) in a system with 26 and 726 neighbors, respectively, are the best for achieving the optimal accuracy [27], [28] (Fig. 12).

Further, we attempted to achieve as many experimental results as possible based on the most commonly used depth cameras, which are Kinect v1 and v2. The depth sensor in Kinect v1 uses the "Light Coding" method that reads the emitted infrared (IR) patterns and obtains depth information from the pattern distortion. For this reason, the depth sensor was divided into an IR projector that emits an IR pattern (left) and an IR camera that reads the pattern (right). A color camera was mounted between the depth sensors [29].

Figure 12. Our algorithm randomly selects a set of *N* number of pixels in each image and then evaluates the average, median, or minimum of difference distribution between real and virtual depths. Furthermore, we select the average, median, or minimum of evaluation values in *M* images. These two randomizations escape from local minima of 6D motion space in our 2D DDM (Source: Watanabe [28] (2015)).

The depth sensor of Kinect v2 employs the "ToF (Time of Flight)" method, which obtains the depth information since the emitted IR light is reflected and returned. The depth sensor, which is not visible from the outside, is equipped with an IR camera (left) and a projector (right) that emits pulse-modulated IR light next to the color camera [30].

Presently, we are testing the performance for developing depth sensor, RealSense D435, based on depth sensor, RealSense R300, which were broken down well. The Intel RealSense Depth Camera D400 series is a stereo vision depth camera that can measure depth. Equipped with two depth sensors, an RGB sensor, and an IR projector, it operates with a USB power supply. The D435 used in this study has a global shutter and a wide viewing angle, providing high-resolution depth information when a moving object must be measured or when the device itself moves. It also minimizes blind spots and covers a larger area than the previous versions.

In a real open surgery, an organ is always obstructed by a patient's body. Therefore, only a part of the organ can be captured by the sensor. For this reason, a real organ should be followed by its virtual organ via the part of surface. In general, when a surgeon cuts an organ, a complicated shape is achieved. With the support of the complicated concave shape, the quality following a virtual organ with its real one increases. Therefore, even if the open part is very narrow, the quality of following improves in our navigation system [31]-[33] (Fig. 13).

In our proposed system, we used the steepest descendent algorithm based on DDM change in the digitalized 6D space defined by three translational DOF and three rotational DOF. Next, in order not to enter into a local minimum, we use the simulated annealing algorithm [34].

However, recently, the digitalized 6D potential field was determined to reach the global minimum without any local minima in a wider area [35]. Owing to this global property, the steepest descendent algorithm always selects the coincidence point between real and virtual organs with respect to three-DOF position and three-DOF orientation.

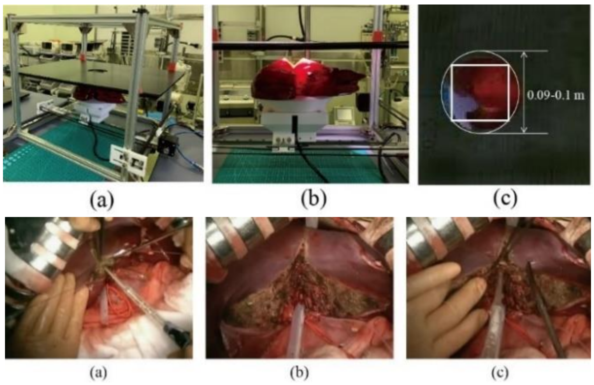

Figure 13. Upper: (a), (b), (c) Strobe shot of actual liver surgery video. Bottom: Occlusion situation. (a) The whole experimental apparatus and (b) the figure which shows the experimental apparatus from the side. The height from the highest part of the liver to the occlusion is 0.02 m. (c) A view of the experimental apparatus from directly above. The occlusion was made from a black plastic board cut out from a 0.1 m or 0.09 m diameter circle, and the initial position of the depth images of the incised real and virtual livers was adjusted using the rectangle inscribed in the occlusion circle (Source: Asano [33] (2020)).

Moreover, the liver is a rheology object with nonlinear viscous and elastic properties. Therefore, it is flexibly deformed and its position/orientation is quickly changed during surgery [37]. Dealing with such a rheological object is difficult, and requires the use of computer graphics in virtual reality, mixed reality, and augmented reality.

As mentioned earlier, we recently determined that the digital search function for the superposition point is globally unimodal (Fig. 14). Accordingly, we constructed an intra-operative surgery navigator that accurately superimposes the virtual and real organs not only with respect to position/posture but also its shape.

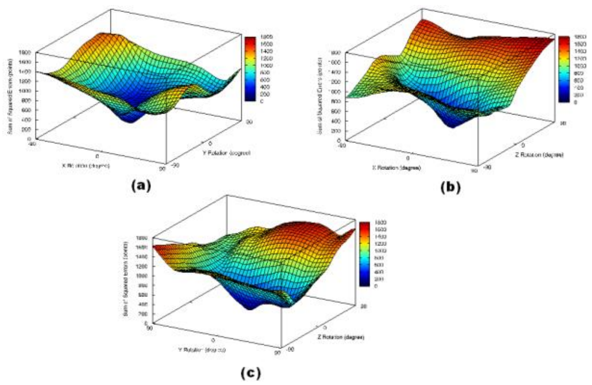

Figure 14. Digital potential field defined by (a) XY rotational DOF, (b) XZ rotational DOF, and (c) YZ rotational DOF. All field shapes are simply concave whose bottom is the coincident point, where the real organ overlaps its virtual counterpart (Source: Numata [35] (2019)).

As shown in Fig. 14, the steepest descent method based on DDM is relatively stable in position/orientation identification. In our surgical navigation, the sampling time, which consists of sensing (e.g., 90 fps for RealSense D435), matching, and investing, is too small; therefore, the shape deformation is also very small. For these reasons, deformation matching according to DDM can be achieved after that. The investigation may sometimes be conducted using a multicore GPU (Fig. 15).

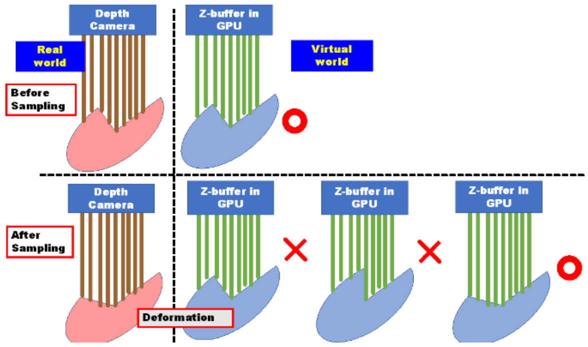

Figure 15. Organ deformation matching by DDM after organ position/orientation matching was finished by DDM.

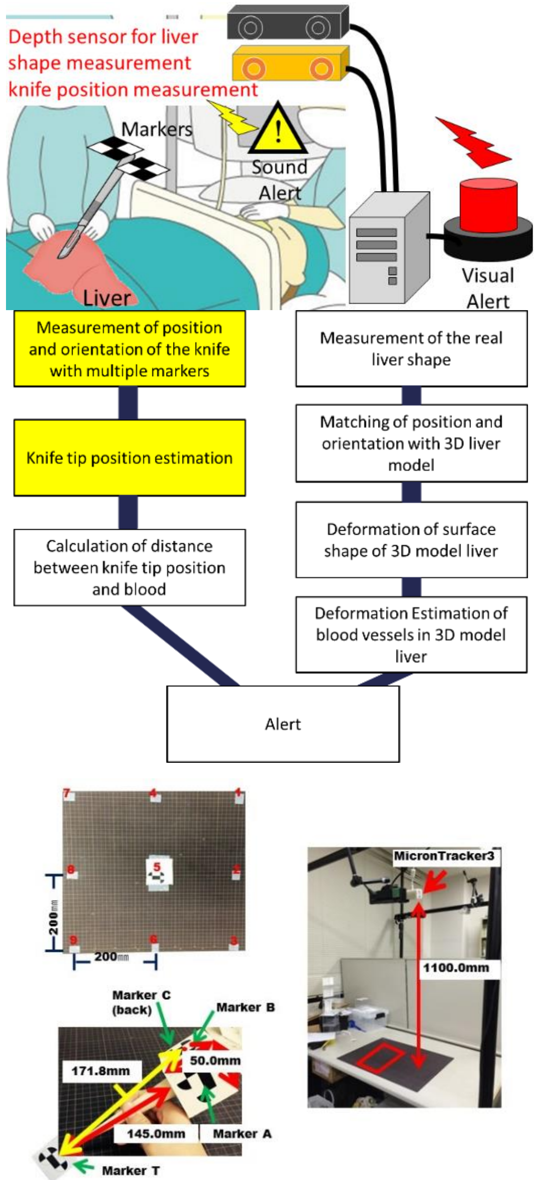

Figure 16. Overall surgical navigation system with a scraper, which is calibrated by many precise artificial landmarks captured by Micron Tracker 3 (Source: Doi [38] (2015)).

Finally, to design an organ surgical navigation system, we calibrated the virtual and real livers as well as the virtual and real Cavitron Ultrasonic Surgical Aspirator (CUSA) scalpels (Fig. 16). In the first stage, we used MicronTracker 3 provided by ClaroNav Co. to identify several special artificial markers [38]-[40]. However, as the marker tracing vision system is extremely expensive, in the second stage of our experiments, we used the ArUco Markers instead [41], [42].

VI. Conclusion

In this paper, we provide a brief history of the organ orientation, position, and shape matching. Since its introduction in 1833, the 3D stereo vision structure has been installed with two cameras to obtain two views by using only one camera and one motion. Because the images and motions have a few errors, we used some digital filter to cancel such noises.

By using this mathematical technique, we acquire SLAM (Simultaneous Localization and Mapping) since 1986. To overlap many point clouds captured from many cameras, researchers used ICP of the PCM. However, as the number of cloud points is extensive, combinatorial calculation was employed to minimize the sum of Euclidean distances between two cloud points. In addition, a target object, such as an organ, cannot be omnidirectionally captured from multiple cameras during a surgery.

Therefore, in 2014, the DDM approach was proposed to match a real organ with its virtual organ. This approach is based on one view and does not have any combination and multiplication calculation. In this paper, we explained many algorithms and experimental extensions of the DDM approach. Finally, we briefly introduced our DDM-based surgical navigation system.

VII. Future Works

In our algorithm, which is based on depth matching and steep descendent method, a part of the object shape is used as a landmark. These landmarks are used to accurately identify the translational and rotational motion of the organ. Typically, in surgical navigation, the cut shape of an organ is used as this landmark. Since artificial landmarks would be a burden to the organ after surgery, we believe their use is impractical.

In addition, the mathematics of the camera is based on linear algebra, so it is not affected by errors in the internal and external parameters of the camera except for random noise. This is because even in the presence of those errors, the zoom in and out will always be nearly linear, and the shape properties useful for matching will be preserved. Therefore, the algorithm does not necessarily require strict camera calibration. Therefore, the algorithm can be applied directly to depth images from pre-calibrated cameras, such as commercial depth/RGB cameras from Microsoft, Intel, etc. (Azure Kinect DK, RealSense L515, D455, D415, ZED 2, etc.). The depth image can be applied as is. The depth image is captured using the times of fright (ToF) or the active stereo principle, but it is not bound by it.

Furthermore, if our algorithm is fast enough, for example, if it supports multiple cores of GPGPU, the sampling time of our algorithm will be within the sampling time of commercial depth/RGB cameras. In such a case, the deformation of the landmarks cannot be neglected because a part of the object shape is slightly deformed. Therefore, the identification of translational and rotational motions of organs during surgery is stable.

In future, these characteristic properties are ascertained by several experiments based on different commercial depth/RGB cameras from Microsoft, Intel, etc. (Azure Kinect DK, RealSense L515, D455, D415, ZED 2, etc.).

Conflict of Interest

The authors declare no conflict of interest.

Author Contributions

Hiroshi Noborio, Katsuhiko Onishi, Masanao Koeda and Miho Asano contributed to the research concept and design; Hiroshi Noborio, Katsuhiko Onishi and Masanao Koeda conceived the project and the study hypothesis; Katsuhiko Onishi, Masanao Koeda and Kaoru Watanabe designed software (including programming) and hardware such as AR (Augmented Reality), CV (Computer Vision), algorithm with programming, respectively; Katsuhiko Onishi, Masanao Koeda and Miho Asano tested the software and hardware, analyzed the data executed from them; Hiroshi Noborio, Masanao Koeda and Miho Asano checked the data; Hiroshi Noborio analyzed and evaluated the data; Hiroshi Noborio clearly wrote the paper by manuscript rewriting; all authors have approved the final version.

Acknowledgment

This study was partly supported by 2014 Grants-in-Aid for Scientific Research (B) (No. 26289069) and 2017 Grants-in-Aid for Scientific Research (C) (No. 17K00420) from the Ministry of Education, Culture, Sports, Science, and Technology, Japan. Further support was provided by the 2014 Cooperation Research Fund from the Graduate School at Osaka Electro-Communication University. Finally, we would like to thank Editage (www.editage.com) for English language editing.

References

[1] Wikipedia. Plastic survey. [Online]. Available: https://en.wikipedia.org/wiki/Plastic_surgery

[2] A. DiGioia, B. Jaramaz, F. Picard, and L. P. Nolte, *Computer and Robotic Assisted Hip and Knee Surgery*, New York: Oxford University Press, 2004.

[3] Wikipedia. Neuronavigation. [Online]. Available: https://en.wikipedia.org/wiki/Neuronavigation

[4] Wikipedia. 3D_stereo_view. [Online]. Available: https://en.wikipedia.org/wiki/3D_stereo_view

[5] Wikipedia. Simultaneous_localization_and_mapping. [Online]. Available: https://en.wikipedia.org/wiki/Simultaneous_localization_and_mapping

[6] R. C. Smith and P. Cheeseman, "On the representation and estimation of spatial uncertainty," *The International Journal of Robotics Research*, vol. 5, no. 4, pp. 56-68, 1986.

[7] J. J. Leonard and H. F. D. Whyte, "Simultaneous map building and localization for an autonomous mobile robot," in *Proc. IROS'91 IEEE/RSJ International Workshop*, Osaka, 1991, pp. 1442-1447.

[8] A. J. Golby, *Image-Guided Neurosurgery*, Academic Press, 2015.

[9] S. Pieper, M. Halle, and R. Kikinis, "3D slicer," in *Proc. the 1st IEEE International Symposium on Biomedical Imaging: From Nano to Macro*, Arlington, 2004, pp. 632-635.

[10] R. Smith and P. Cheeseman, "On the representation and estimation of spatial uncertainty," *Int. J. Robotics Research*, vol. 5, no. 4, pp. 56-68, 1986.

[11] R. A. Brooks, "Visual map making for a mobile robot," in *Proc. IEEE Int. Conf. Robotics and Automation*, St. Louis, 1985, pp. 824-829,

[12] R. Chatila and J. P. Laumond, "Position referencing and consistent world modeling for mobile robots," in *Proc. IEEE Int. Conf. Robotics and Automation*, St. Louis, 1985, pp. 138-145,

[13] R. M. Artal and J. D. Tardós, "ORB-SLAM2: An open-source SLAM system for monocular, stereo and RGB-D cameras," *IEEE Transactions on Robotics*, vol. 33, no. 5, pp. 1255-1262, 2017.

[14] K. Konolige and G. R. Bradski, "An efficient alternative to SIFT or SURF," in *Proc. the 2011 International Conference on Computer Vision*, 2011, pp. 2564-2571.

[15] M. Koeda, S. Nishimoto, H. Noborio, and K. Watanabe, "Proposal and evaluation of AR-based microscopic brain surgery support system," in *Human-Computer Interaction. Recognition and Interaction Technologies*, M. Kurosu, Ed., Orlando: Springer, 2019, pp. 438-446.

[16] Wikipedia. Iterative_closest_point. [Online]. Available: https://en.wikipedia.org/wiki/Iterative_closest_point

[17] Y. Chen and M. Gerard, "Object modelling by registration of multiple range images," *Image Vision Comput*., vol. 10, no. 3, pp. 145-155, 1991.

[18] P. J. Besl and N. D. McKay, "A method for registration of 3-D shapes," *IEEE Trans. Pattern Anal. Mach. Intell.*, vol. 14, no. 2, pp. 239-256, 1992.

[19] Z. Zhang, "Iterative point matching for registration of free-form surfaces," *Int. Journal of Computer Vision*, vol. 13, no. 2, pp. 119-152, 1994.

[20] S. Granger and X. Pennec, "Multi-scale EM-ICP: A fast and robust approach for surface regis-tration," in *Proc. 7th European Conference on Computer Vision*, 2002, pp. 69-73,

[21] Y. Liu, "Automatic registration of overlapping 3D point clouds using closest points," *Journal of Image and Vision Computing*, vol. 24, no. 7, pp. 762-778, 2006.

[22] J. Salvi, C. Matabosch, D. Fofi, and J. Forest, "A review of recent range image registration methods with accuracy evaluation," *Journal of Image and Vision Computing*, vol. 25, no. 5, pp. 578-596, 2007.

[23] R. B. Rusu and S. Cousins, "3D is here: Point Cloud Library (PCL)," in *Proc. IEEE Int. Conf. Robotics and Automation*, 2011, pp. 1-4.

[24] Y. F. Wu, W. Wang, K. Q. Lu, Y. D. Wei, and Z. C. Chen, "A new method for registration of 3D point sets with low overlapping ratios," in *Proc. 13th CIRP conference on Computer Aided Tolerancing*, 2015, pp. 202-206.

[25] H. Noborio, K. Onishi, M. Koeda, K. Mizushino, M. Yagi, M. Kaibori, *et al.*, "Motion transcription algorithm by matching corresponding depth image and Z-buffer," in *Proc. the 10th Anniversary Asian Conference on Computer Aided Surgery*, Kyusyu University, Fukuoka Japan, 2014, pp. 60-61.

[26] H. Noborio, K. Watanabe, M. Yagi, Y. Ida, K. Onishi, M. Koeda, *et al.*, "Image-based initial position/orientation adjustment system between real and virtual livers," *Jurnal Teknologi: Medical Engineering*, vol. 77, no. 6, pp. 41-45, 2015.

[27] K. Watanabe, M. Yagi, K. Ota, K. Onishi, M. Koeda, S. Nankaku, *et al.*, "Parameter identification of depth-depth-matching algorithm for liver following," *Jurnal Teknologi: Medical Engineering*, vol. 77, no. 6, pp. 35-39, 2015.

[28] K. Watanabe, M. Yagi, A. Shintani, S. Nankaku, K. Onishi, M. Koeda, *et al.*, "A new 2D depth-depth matching algorithm whose translation and rotation freedoms are separated," in *Proc. of the International Conference on Intelligent Informatics and Biomedical Sciences (ICIIBMS2015), Track 3: Bioinformatics, Medical Imaging and Neuroscience*, Okinawa, Japan, 2015, pp. 271-278.

[29] H. Noborio, K. Watanabe, M. Yagi, Y. Ida, S. Nankaku, K. Onishi, *et al.*, "Experimental results of 2D depth-depth matching algorithm based on depth camera kinect v1," *Journal of Bioinformatics and Neuroscience*, vol. 1, no. 1, pp. 38-44, 2015.

[30] H. Noborio, K. Watanabe, M. Yagi, Y. Ida, S. Nankaku, K. Onishi, *et al.*, "Tracking a real liver using a virtual liver and an experimental evaluation with kinect v2," in *Proc. of the 4th International Work-Conference on Bioinformatics and Biomedical Engineering*, Granada, Spain, 2016, pp.149-162.

[31] K. Watanabe, M. Yagi, K. Onishi, M. Koeda, H. Noborio, and M. Kaibori, "Evaluation of depth-depth matching algorithm for following human liver whose motion is practical and also is occluded by human body," in *Proc. of the 10th MedViz Conference and the 6th Eurographics Workshop on Visual Computing for Biology and Medicine*, Bergen, Norway, 2016, pp. 135-138.

[32] M. Asano, T. Kuroda, S. Numata, T. Jozen, T. Yoshikawa, and H. Noborio, "Convergence stability of depth-depth-matching-based steepest descent method in simulated liver surgery," *International Journal of Pharma Medicine and Biological Sciences*, to appear.

[33] M. Asano, T. Kuroda, S. Numata, T. Jozen, T. Yoshikawa, and H. Noborio, "Stability maintenance of depth-depth matching of steepest descent method using an incision shape of an occluded organ," in *Human-Computer Interaction. Human Values and Quality of Life*, M. Kurosu, Ed., Springer, 2020, pp. 539-555,

[34] H. Noborio, S. Yoshida, K. Watanabe, D. Yano, and M. Koeda, "Comparative study of depth-image matching with steepest descendent and simulated annealing algorithms," in *Proc. of the 11th International Joint Conference on Biomedical Engineering Systems and Technologies*, 2018, pp. 77-87.

[35] S. Numata, M. Koeda, K. Onishi, K. Watanabe, and H. Noborio, "Performance and accuracy analysis of 3D model tracking for liver surgery," in *Human-Computer Interaction. Recognition and Interaction Technologies*, M. Kurosu, Ed., Springer, 2019, pp. 524-533.

[36] H. Noborio, K. Onishi, M. Koeda, K. Mizushino, T. Kunii, M. Kaibori, *et al.*, "Fast surgical algorithm for cutting with liver standard triangulation language format using Z-buffers in graphics processing unit," in *Computer Aided Surgery*, M. Fujie, Ed., Japan: Springer, 2016, pp. 127-140.

[37] H. Noborio, K. Watanabe, M. Yagi, K. Takamoto, S. Nankaku, K. Onishi, *et al.*, "Depth image matching algorithm for deforming and cutting a virtual liver via its real liver captured by kinect v2," in *Proc. of the 4th International Work-Conference on Bioinformatics and Biomedical Engineering*, Granada, Spain, 2016, pp. 196-205.

[38] M. Doi, D. Yano, M. Koeda, H. Noborio, K. Onishi, M. Kayaki, *et al.*, "Knife tip position estimation using multiple markers for Liver surgery support," in *Proc. of the 6th International Conference on Advanced Mechatronics*, Tokyo, Japan, 2015, pp. 74-75.

[39] D. Yano, M. Koeda, M. Doi, K. Okumoto, S. Yoshida, K. Onishi, *et al.*, "Accuracy verification of knife tip positioning with position and orientation estimation of the actual liver for liver surgery support system," *Journal of Bioinformatics and Neurosciences*, vol. 3, no. 3, pp.79-84, 2017.

[40] M. Koeda, D. Yano, M. Doi, K. Onishi, and H. Noborio, "Calibration of surgical knife-tip position with marker-based optical tracking camera and precise evaluation of its measurement accuracy," *International Journal of Bioinformatics and Neuroscience*, vol. 4, no. 1, pp. 155-159, 2018.

[41] Detection of ArUco markers. [Online]. Available: https://docs.opencv.org/trunk/d5/dae/tutorial_aruco_detection.html

[42] S. G. Jurado, R. M. Salinas, F. J. M. Cuevas, and M. J. M. Jiménez, "Automatic generation and detection of highly reliable fiducial markers under occlusion," *Pattern Recogn.*, vol. 47, no. 6, pp. 2280-2292, 2014.

Hiroshi Noborio graduated from the Department of Computer Science, Shizuoka University, Hamamatsu, Japan, and received the Dr.Eng. degree from the Department of Mechanical Engineering, Faculty of Engineering Science, Osaka University, Toyonaka, Japan. From 1987 to 1988, Noborio was an Assistant Professor at Osaka University. From 1988, he joined as a lecturer at Osaka Electro-Communication University. Professor Noborio was the Dean of the Faculty of Information Science and Arts in OECU from 2009 to 2012, and is currently a Professor at the Department of Computer Science. His research interests include surgical simulation and navigation in the medical and dental areas. Dr. Noborio is a member of IEEE, RSJ, SICE, IPSJ, and IEICE.

Katsuhiko Onishi received the B.E., M.E., and Ph.D. degrees from Osaka University in 1998, 2000, and 2005, respectively. From 2002 until 2006, he was an Assistant Professor at the Graduate School of Information Science and Technology, Osaka University. Since April 2006, he has been working as an Associate Professor, and then he is currently a Professor at the Department of Computer Science, Osaka Electro-Communication University. His research interests include 3D user interface and human-computer interaction.

Masanao Koeda graduated from the Department of Mechanical Engineering, Faculty of Engineering Science, Osaka University, Toyonaka, Japan in 2000. He received the Dr. Eng. degree from the Division of Information Science, Nara Institute of Science and Technology, Nara, Japan in 2005. From 2005 to 2008, he was a lecturer at the Department of Human and Computer Intelligence, Ritsumeikan University. Since 2008, he has been employed as an associate professor at the Osaka Electro-Communication University. He is currently an associate professor at the Faculty of Computer Science and Systems Engineering, Department of Human Information Engineering, Okayama Prefectural University. His research interests include computer vision in surgical simulation and navigation, and Robotics. He is a member of IEEE, RSJ, IPSJ, and VRSJ.

Kaoru Watanabe graduated from the Department of Computer Science, Niigata University, Niigata, Japan, and received the Dr.Eng. degree from the Department of Computer Science, Niigata University, Niigata, Japan in 1986. From 1987 to 2003 and 2004 to 2005, he worked as a Lecturer and an Associate Professor at the Department of Engineering Informatics, Neyagawa, respectively. Currently, he is a Professor at the Department of Computer Science, Shijo-Nawate, in Osaka Electro-Communication University. His research interests include algorithms of surgical simulation and navigation. Professor Watanabe is a member of IEEE, IPSJ, and IEICE.

Miho Asano graduated from the Graduate School of Arts and Sciences, The Open University of Japan, Chiba, Japan and enrolled at the Graduate School of Engineering Science, Osaka University, Toyonaka, Japan from 2016 to 2018. Since 2016, Asano has been a research assistant at the Preemptive Medicine & Lifestyle-Related Disease Research Center of Kyoto University Hospital. She is interested in biomedical engineering, brain function measurement, National Databases, and surgical navigation systems.